Chemical Geology 618 (2023) 121293

Contents lists available at ScienceDirect

Chemical Geology

journal homepage: www.elsevier.com/locate/chemgeo

Cadmium isotope fractionation during metal-silicate partitioning – Results and implications for Earth's volatile accretion

Harvey Pickard [a], Emeliana Palk [a,b], Bernard J. Wood [c], Mark Rehkämper [a,*]

[a] Department of Earth Science & Engineering, Imperial College London, London SW7 2AZ, UK
[b] School of Earth Sciences, University of Bristol, Bristol BS8 1RJ, UK
[c] Department of Earth Sciences, University of Oxford, South Parks Road, Oxford OX1 3AN, UK

ARTICLE INFO

Editor: S Aulbach

Keywords:
Cadmium
Cd isotopes
Metal-silicate partitioning
Isotope fractionation
Volatile depletion
Bulk silicate Earth
Core formation

ABSTRACT

Metal-silicate partitioning experiments were carried out at 1.5 GPa and 1508 to 1843 K to constrain Cd partitioning and isotope fractionation during core formation. At the studied conditions, there was no significant stable isotope fractionation during Cd partitioning between metal and silicate phases with a mean $\Delta^{114}Cd_{met\text{-}sil} = -0.02 \pm 0.09$‰ (2SD, $n = 7$). Two experiments that investigated sulphide-silicate partitioning of Cd yielded fractionation factors of -0.04 ± 0.06‰ and -0.23 ± 0.07‰ (2SE), whereby the latter result was obtained for a short run that may not represent full equilibrium. In summary, the findings suggest that Cd isotope fractionation during segregation of Earth's core was either absent or very minor. The Cd partitioning data of this and previous investigations were combined in multiple linear regression analyses to better constrain Cd metal-silicate partitioning during core formation. In accord with earlier work, the analyses reveal that Cd metal-silicate partitioning is not significantly impacted by temperature and pressure but affected by the S content of the metal phase. In addition, it is shown that the presence of C and Si in the metal reduce the siderophile character of Cd. Based on estimates for the composition of Earth's core, the data suggest a metal-silicate partition coefficient D_{Cd} of about 0.4 for a single-stage core formation event. However, given uncertainties about the light element composition of Earth's core, D_{Cd} values larger than 1 cannot be ruled out at present for core formation. The results of this study and data on the composition of the bulk silicate Earth and chondritic meteorites were applied in mass balance calculations to constrain the Cd signature of Earth's main stage accretion material prior to delivery of the late veneer. The modelling indicates Earth's main stage of accretion involved material with an average Cd isotope composition that was lighter than that of known carbonaceous and enstatite chondrites. Most likely, this reflects either poor characterisation of these meteorites by the few precise data currently available or that a significant fraction of the terrestrial volatile inventory was acquired from material not directly related to carbonaceous and enstatite chondrites. Furthermore, terrestrial accretion most likely did not encompass the addition of a volatile-rich late veneer exceeding 2% of Earth's mass, in accord with accretion models, which invoke that volatile delivery occurred primarily during main stage accretion, alongside core formation.

1. Introduction

Both the Earth and chondritic meteorites display variable volatile element depletions relative to bulk solar system abundances, as approximated by CI chondrites and the solar photosphere (Palme and O'neill, 2014; Palme et al., 2014; Braukmüller et al., 2018; Braukmüller et al., 2019). Analyses of mantle peridotites give some indication about the origin and extent of Earth's volatile depletion. This approach, however, also requires some knowledge of accretionary processes, and the effect they had on the abundance patterns and isotope compositions of volatile elements. Specifically, volatile element abundances and isotope compositions of Earth's mantle should reflect the combined effects of volatile depletion of the material that accreted to form Earth in the protosolar disk, metal-silicate partitioning during core segregation, and any additional processes that affected volatile abundances during terrestrial accretion.

Previous studies debated the mechanism by which Earth accreted volatile elements and the role played by the late veneer (e.g., Albarède, 2009; Wood et al., 2010). The late veneer hypothesis was initially proposed to explain the chondritic relative abundances of highly

* Corresponding author.
E-mail address: markrehk@imperial.ac.uk (M. Rehkämper).

https://doi.org/10.1016/j.chemgeo.2022.121293
Received 5 March 2022; Received in revised form 12 December 2022; Accepted 23 December 2022
Available online 25 December 2022

siderophile elements (HSE) in the terrestrial mantle (Chou, 1978), which exceed predictions based on core-mantle partitioning (Mann et al., 2012). Whilst it has also been suggested that the HSE systematics of Earth's mantle reflect incomplete core formation or reduced siderophile behaviour of the HSE at high pressure and temperature, they are most readily explained by invoking a late influx of chondritic material, equating to roughly 0.5% of Earth's mass (M_E) after the formation of Earth's core (Holzheid et al., 2000; Walker, 2009). This 'classical' model of volatile accretion predicts that most of Earth's volatile elements were acquired during main stage accretion whilst core formation was ongoing. In this case volatile addition may have occurred either throughout Earth's formation or, according to heterogeneous accretion models, primarily during the late stages of the main accretion process, when Earth assimilated volatile-rich carbonaceous planetesimals (e.g., Schönbächler et al., 2010; Wade et al., 2012; Braukmüller et al., 2019; Budde et al., 2019; Righter et al., 2020; Kubik et al., 2021). In this case, the late veneer only dominates the mantle abundances of the most siderophile elements. Alternative models invoke a much larger late veneer, and with a volatile-rich composition this can be Earth's main volatile source. In particular, Albarède (2009) suggested a 2–5% M_E late veneer comprised of volatile-rich CI chondrites, whilst later work successfully modelled the $^{238}U/^{204}Pb$ and Rb/Pb ratios of the modern mantle via addition of a 2.5% M_E late veneer of CI chondritic composition to a refractory proto-Earth (Ballhaus et al., 2013). Wood et al. (2010) disputed such a large late veneer, as such accretion scenarios would establish higher abundances of highly siderophile and volatile elements in the silicate Earth than are currently observed and because volatile siderophile elements are depleted in the bulk silicate Earth relative to similarly volatile lithophile elements, and so must have already been present in the Earth during core formation.

Cadmium is a highly volatile element with a 50% condensation temperature of 502 K (Wood et al., 2019), which displays siderophile and chalcophile tendencies. Many metal-silicate partitioning experiments, carried out over a wide range of temperatures (1700 to 2800 K) and pressures (1 to 20 GPa) find Cd to be moderately siderophile, with a metal-silicate partition coefficient (D_{Cd}) generally between 1 and 20 (Ballhaus et al., 2013; Wang et al., 2016; Righter et al., 2018; Steenstra et al., 2017; Steenstra et al., 2020a, 2020b). Whilst most previous investigations concluded that both temperature and pressure have no resolvable effect on Cd metal-silicate partitioning (Kiseeva and Wood, 2015; Kubik et al., 2021) there are a few studies which claim Cd is increasingly siderophile at higher temperatures (Ballhaus et al., 2013; Steenstra et al., 2020b). Most of the latter results were, however, obtained in very short experiments that may have not reached full chemical equilibrium. Also of significance are the effects that elements such as S, C, and Si have on Cd partitioning, given that they may contribute significantly to the light element budget of Earth's core (Wang et al., 2018). Importantly, D_{Cd} values were found to be enhanced for experiments in which the metal phase contained appreciable S, with some experiments exhibiting D_{Cd} values of about 200 (Lagos et al., 2008; Kiseeva and Wood, 2013; Wood et al., 2014; Kiseeva and Wood, 2015; Righter et al., 2018; Steenstra et al., 2020a; Kubik et al., 2021). Conversely, metal-silicate partition coefficients for Cd were generally lower in experiments where the metal phase contained C (Lagos et al., 2008; Righter et al., 2018), Si (Righter et al., 2019; Steenstra et al., 2020b), and possibly O (Kiseeva and Wood, 2015).

To better constrain the origin of Earth's volatiles, a recent investigation determined the Cd stable isotope composition of the BSE, and this was estimated to be isotopically lighter than enstatite and carbonaceous chondrites (Pickard et al., 2022). This implies that the Cd isotope composition of the BSE was either fractionated during accretion or that Earth's Cd inventory was not only acquired from material related to known carbonaceous and enstatite chondrites. A key process that can fractionate Cd isotopes during accretion is metal-silicate partitioning during core segregation. Furthermore, observations from natural hydrothermal settings and laboratory experiments show that sulphide phases preferentially incorporate light Cd isotopes at low temperatures. This suggests that such isotope fractionation may also occur during segregation of S-rich metallic liquids during core formation (Schmitt et al., 2009; Guinoiseau et al., 2018; Xie et al., 2019). As Cd isotope fractionation during Earth's differentiation has hitherto not been investigated, the current study addresses this issue through experimental studies that examine the extent of stable Cd isotope fractionation during metal-silicate partitioning. These results and literature data are further employed with the aid of multiple linear regression analyses and Monte Carlo mass balance models, to determine the mean Cd concentration and isotope composition of Earth's main stage accretion material and assess the origin of Earth's volatile inventory from a new angle.

2. Metal-silicate partitioning experiments

The metal-silicate partitioning experiments were carried out in a similar manner to those of Wood et al. (2014). The starting materials consisted of Fe metal or sulphide and a silicate component, in approximately equal proportions by weight, plus 0.4 to 1.0 wt% CdO in the silicate. The silicate component had a composition close to the anorthite-diopside-forsterite eutectic at 1.5 GPa (Presnall et al., 1978) and was prepared by mixing reagent grade SiO_2, MgO, Al_2O_3 and $CaCO_3$ in the correct proportions. The mixture was heated slowly from 500 °C to 1000 °C to decarbonate the $CaCO_3$, then re-ground and fired at 1200 °C for 1 h. A sodium disilicate component (formed from reagent-grade Na_2CO_3 and SiO_2 at 1 atm), and a minor FeO component were added to the time series experiments to reduce the CMAS (CaO-MgO-Al_2O_3-SiO_2) liquidus temperature (Gudfinnsson and Presnall, 2000; Heber et al., 2007; Walter and Presnall, 1994) and limit volatile loss of Cd and associated kinetic isotope fractionation.

All experiments were performed at 1.5 GPa, using a 12.7 mm inside diameter end-loaded piston-cylinder apparatus at the Department of Earth Sciences, University of Oxford. Powdered samples were loaded into 6 mm outside diameter, 3 to 4 mm inside diameter capsules made either of SiO_2 glass, polycrystalline MgO or graphite. The 5 mm long capsules were centred in an 8 mm outside diameter, 6 mm inside diameter, 30 mm long graphite furnace with crushable MgO pieces situated above and below the capsule. A type C thermocouple was introduced into the assembly through the MgO spacer from above and situated on top of the capsule but separated from it by a protective 0.5 mm thick alumina disk. External to the cylindrical graphite furnace were cylinders of SiO_2 glass (1 mm thick) next to the furnace and pyrophyllite next to the pressure plate.

Three sets of experiments are presented in this study (Table 1). The first set (BW1305 to BW1308) investigates the effects of temperature and capsule composition on Cd partitioning and isotope fractionation. These experiments were run with silica, graphite and MgO capsules at 1643 to 1843 K for 56 to 70 min, consistent with equilibrium partitioning in capsules of this size (Tuff et al., 2011). The second set of experiments (BW1517 to BW1521) was carried out in graphite capsules at 1508 K, with run durations that varied from 4 to 200 min. Finally, experiments BW1522 and BW1523 were also conducted in graphite capsules at 1508 K and investigated the partitioning of Cd between Fe sulphide and silicate melt in runs of 41 and 15 min, respectively.

On completion, the experiments were quenched by cutting the power to the graphite furnace whilst maintaining experimental pressure, before gradually decompressing the sample. Quenched experimental products were composed of solidified Fe metal that coalesced into a single or several metal balls, encased in silicate glass or a mixture of glass and quench olivine crystals. Fig. 1 shows a back-scattered electron image of run products from a metal-silicate partitioning experiment carried out under similar conditions and with exactly the same (graphite) capsule arrangement as that used for many of the experiments described here. As can be seen, there is excellent segregation of metal from silicate, with the former forming mm-sized balls at the centre of the capsule, and no evidence for the presence of significant metal nuggets within the silicate.

Table 1
Cd isotope compositions, concentrations and partition coefficients determined for experimental run products and experimental run conditions.

	BW1305	BW1306	BW1307	BW1308	BW1517	BW1518
Capsule	Silica	Graphite	MgO	Graphite	Graphite	Graphite
Starting Materials	49% CMAS + 1% CdO + 50% Fe	49% CMAS + 1% CdO + 50% Fe	49% CMAS + 1% CdO + 50% Fe	26% CMAS + 26% $Na_2Si_2O_5$ + 1% CdO + 47% Fe	20% CMAS + 30% $Na_2Si_2O_5$ + 0.4% CdO + 45% Fe + 5% FeO	20% CMAS + 30% $Na_2Si_2O_5$ + 0.4% CdO + 45% Fe + 5% FeO
Temperature (K)	1838	1713	1843	1643	1508	1508
Duration (mins)	58	56	63	70	66	12
$[Cd]_{metal}$ (μg/g)	33	11,416	164	12,018	2258	3452
$[Cd]_{silicate}$ (μg/g)	18	6605	47	3283	4307	4193
$D_{Cd\ (met/sil)}$	1.8 ± 0.1	1.7 ± 0.1	3.5 ± 0.7	3.7 ± 0.3	0.52 ± 0.03	0.82 ± 0.16
K_D (Cd)	0.07 ± 0.01	0.15 ± 0.02	0.13 ± 0.04	0.23 ± 0.02	0.08 ± 0.01	–
$\delta^{114}Cd_{metal}$	+1.13 ± 0.07	+0.05 ± 0.07	+2.93 ± 0.07	+0.01 ± 0.06	−0.03 ± 0.05	+0.01 ± 0.04
$\delta^{114}Cd_{silicate}$	+1.09 ± 0.08	+0.01 ± 0.07	+2.96 ± 0.08	+0.04 ± 0.06	+0.06 ± 0.05	+0.07 ± 0.04
$\Delta^{114}Cd_{met\text{-}sil}$	+0.04 ± 0.10	+0.04 ± 0.10	−0.03 ± 0.11	−0.02 ± 0.09	−0.09 ± 0.07	−0.05 ± 0.06

	BW1519	BW1520	BW1521	BW1522	BW1523
Capsule	Graphite	Graphite	Graphite	Graphite	Graphite
Starting Materials	20% CMAS + 30% $Na_2Si_2O_5$ + 0.4% CdO + 45% Fe + 5% FeO	20% CMAS + 30% $Na_2Si_2O_5$ + 0.4% CdO + 45% Fe + 5% FeO	20% CMAS + 30% $Na_2Si_2O_5$ + 0.4% CdO + 45% Fe + 5% FeO	20% CMAS + 30% $Na_2Si_2O_5$ + 0.6% CdO + 45% FeS + 5% FeO	20% CMAS + 30% $Na_2Si_2O_5$ + 0.6% CdO + 45% FeS + 5% FeO
Temperature (K)	1508	1508	1508	1508	1508
Duration (mins)	200	30	4	41	15
$[Cd]_{metal}$ (μg/g)	1265	2256	3507	*6441	*2582
$[Cd]_{silicate}$ (μg/g)	4911	4889	3251	221	144
$D_{Cd\ (met\text{-}sil)}$	0.26 ± 0.02	0.46 ± 0.03	1.1 ± 0.3	**29.1 ± 5.8	**17.9 ± 3.6
K_D (Cd)	–	–	–	–	–
$\delta^{114}Cd_{metal}$	+0.03 ± 0.04	0.00 ± 0.04	0.00 ± 0.05	† − 0.06 ± 0.05	† − 0.03 ± 0.05
$\delta^{114}Cd_{silicate}$	+0.07 ± 0.04	+0.01 ± 0.05	+0.05 ± 0.06	−0.02 ± 0.05	+0.20 ± 0.05
$\Delta^{114}Cd_{met\text{-}sil}$	−0.04 ± 0.06	−0.01 ± 0.06	−0.05 ± 0.08	†† − 0.04 ± 0.06	†† − 0.23 ± 0.07

[Cd] = Cd concentration of the metal and silicate phases. Concentrations denoted by * represent the Cd concentration of the sulphide phase. Metal-silicate partition coefficient for Cd, $D_{Cd\ (met\text{-}sil)} = [Cd]_{metal} / [Cd]_{silicate}$. D_{Cd} values denoted by ** represent sulphide-silicate partition coefficients, $D_{Cd\ (sul\text{-}sil)} = [Cd]_{sulphide} / [Cd]_{silicate}$. Metal-silicate exchange coefficient, K_D (Cd) = $D_{Cd\ (met\text{-}sil)} / D_{Fe\ (met\text{-}sil)}$. Partition coefficient and K_D uncertainties represent propagated 2SD values, mainly from weighing errors associated with low sample masses. The $\delta^{114}Cd$ values are shown relative to the Cd-doped CMAS starting material ($\delta^{114}Cd = -0.11 \pm 0.05$‰ relative to NIST SRM 3108), with Cd isotope uncertainties denoting average within-run 2SE errors. $\delta^{114}Cd_{metal}$ values denoted by † represent the Cd isotope composition of the sulphide phase. Metal-silicate Cd isotope fractionation, $\Delta^{114}Cd_{met\text{-}sil} = \delta^{114}Cd_{metal} - \delta^{114}Cd_{silicate}$. $\Delta^{114}Cd_{met\text{-}sil}$ values denoted by †† represent sulphide-silicate isotope fractionation, $\Delta^{114}Cd_{sul\text{-}sil} = \delta^{114}Cd_{sulphide} - \delta^{114}Cd_{silicate}$. $\Delta^{114}Cd$ uncertainties (2SE) are propagated from $\delta^{114}Cd$ uncertainties.

A spatula blade was employed to physically separate components that were bonded together. The metal and silicate fragments were then hand-picked under an optical microscope to ensure that only pure phases were selected for analysis. Whilst the hand-picking further confirmed the absence of metal nuggets within the silicate grains, a hand magnet was passed over the picked silicates to ensure remove of any stray metal fragments.

3. Analysis of samples from partitioning experiments

3.1. Cd stable isotope compositions

Sample preparation and Cd stable isotope measurements were carried out in the clean room and mass spectrometry facilities of the MAGIC Laboratories at the Department of Earth Science & Engineering, Imperial College London. A detailed account of the methods is provided in recent publications (Murphy et al., 2016; Palk et al., 2018; Pickard et al., 2022) and only a brief summary is given here.

The silicate fractions of the samples produced in the metal-silicate partitioning experiments were digested in 6 ml of a 1 + 2 mixture of 16 M HNO_3 and 28 M HF, whilst the metal fractions were digested in 8 ml of a 1 + 3 mixture of 16 M HNO_3 and 6 M HCl. Both silicate and metal digestion procedures were carried out at 130 °C for 3 to 7 days, before evaporation to dryness and re-dissolution in 20 ml of 6 M HCl. An aliquot of this solution was then mixed and equilibrated with a ^{111}Cd—^{113}Cd double-spike solution (Xue et al., 2012). After this, Cd was separated from the sample matrix with a three-stage column chromatography procedure (Ripperger and Rehkämper, 2007; Xue et al., 2012), followed by extraction of the final Cd fraction with heptane to remove organic resin constituents (Murphy et al., 2016). The Cd yield of the chemical separation ranged from 70 to 100%.

The Cd isotope analyses were carried out with a Nu Plasma HR MC-ICP-MS equipped with standard sampler and skimmer cones. Sample introduction utilised a Cetac autosampler and a Nu Instruments DSN desolvation system equipped with glass or PFA cross-flow nebulisers with nominal uptake rates of 100 μl/min. The ion beams of ^{111}Cd, ^{112}Cd, ^{113}Cd, and ^{114}Cd were monitored for data acquisition, whilst the ^{115}In and ^{117}Sn ion beams were measured for interference corrections, all using Faraday collectors with 10^{11} Ω resistors. Instrumental sensitivity for Cd was typically 200–300 V/(μg ml^{-1}). The sample analyses were carried out with Cd solutions of 80 to 100 ng/ml in 0.1 M HNO_3 interspersed between and relative to analyses of double-spiked solutions of the NIST SRM 3108 Cd isotope reference material with matching elemental concentrations and ratios of spike-derived to natural Cd. The isotope measurements started with a peak centring routine and then encompassed three blocks of data acquisition each with 20 integrations of 5 s, and a preceding 15 s determination of the electronic baselines whilst the ion beam was deflected in the electrostatic analyser. In between runs, the sample introduction system was washed with 0.1 M HNO_3 for at least 120 s. Following the measurements, the reduction of the double spike data was carried out offline using an iterative approach, which corrects for both the monitored isobaric interferences and any laboratory- or instrument-induced mass discrimination (Arnold et al., 2010; Xue et al., 2012).

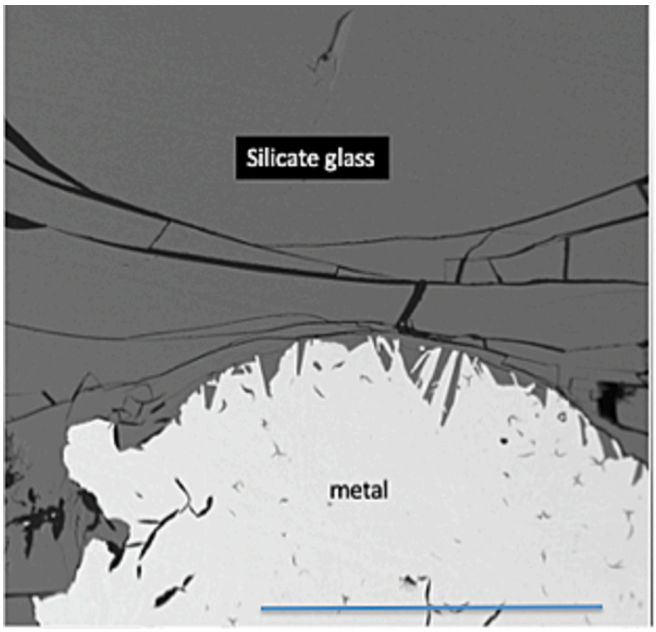

Fig. 1. Backscattered electron image of experiment BW2026 which was performed under similar conditions and with the same size of graphite capsule as that used in this study. Scale bar is 1000 μm. Note excellent segregation of the metal which contains laths of graphite exsolved during the quench.

The stable Cd isotope compositions of the samples were initially determined as δ^{114}Cd values relative to the NIST SRM 3108 Cd isotope reference material (Abouchami et al., 2013):

$$\delta^{114/110}\mathrm{Cd} = \left[\frac{\left(^{114}\mathrm{Cd}/^{110}\mathrm{Cd}\right)_{\mathrm{sample}}}{\left(^{114}\mathrm{Cd}/^{110}\mathrm{Cd}\right)_{\mathrm{NIST\ SRM\ 3108}}} - 1\right] \times 10^3 \quad (1)$$

For convenience, the δ^{114}Cd values for samples from the partitioning experiments are reported and discussed relative to the Cd-doped CMAS starting material (Table 1). The latter material has a Cd isotope composition that is offset from NIST SRM 3108 Cd by $\delta^{114}\mathrm{Cd} = -0.11 \pm 0.05$‰ (2SD; $n = 7$). In contrast, all other δ^{114}Cd data, and in particular literature values for the BSE and meteorites, are quoted relative to SRM 3108 Cd.

The secondary Cd isotope reference material BAM-I012 Cd was routinely analysed alongside samples, yielding $\delta^{114}\mathrm{Cd} = -1.34 \pm 0.07$‰ (2SD; $n = 48$), in accord with previous results (Abouchami et al., 2013; Murphy et al., 2016). During the course of the study, the total Cd blank of the analytical procedure (from digestion to isotope measurement) was as low as 1 pg and about 20 pg on average. At this level, the blanks increased the total Cd content of the samples by <0.002‰. Given the essentially negligible blank contributions, no blank corrections were implemented for the Cd isotope and concentration data. Reported uncertainties for the Cd isotope data (Table 1) represent the average within-run 2SE uncertainties, which were generally marginally larger than the 2SD between-run uncertainties of the bracketing standards. The Cd concentrations of the metal and silicate phases of each experiment were obtained by isotope dilution from the mass bias corrected ^{111}Cd/^{114}Cd ratios of the spiked sample solutions and applied to determine the Cd partition coefficients. The 2SD uncertainties of the latter results were dominated by the weighing errors for the samples (of typically ±0.1 mg) due to the low sample masses.

3.2. Major element concentrations

The major element concentrations (Na, Mg, Al, Si, P, S, Ca, Ti, Mn, and Fe) were determined on small samples of the silicate fractions of the initial experiments (BW1305 to BW1308) and the time series experiment BW1317 to better understand possible compositional effects on Cd partitioning and isotope fractionation, including potential impacts of capsule material dissolution and associated sample contamination. Samples were analysed using a JEOL JXA8600 electron microprobe at the Department of Archaeology, University of Oxford, using methods outlined in Wood et al. (2014).

4. Results

4.1. Metal-silicate partitioning experiments

Table 1 outlines the run conditions for the metal-silicate partitioning experiments, alongside Cd concentration and isotope data, and partitioning behaviour. Major element concentrations for selected experimental charges are available in Table S1 (Supplementary material).

4.1.1. Cadmium metal-silicate partition coefficients

The metal-silicate partition coefficient of Cd represents the ratio of the mass concentrations of Cd in the metal and silicate phases:

$$D_{\mathrm{Cd}} = \frac{[\mathrm{Cd}]_{\mathrm{met}}}{[\mathrm{Cd}]_{\mathrm{sil}}} \quad (2)$$

The same principle is used to assess the partitioning of Cd between sulphide and silicate phases of experiments BW1522 and BW1523. Cadmium appears to display no strong preference for either the metal or silicate phases across all nine of the metal-silicate partitioning experiments (BW1305-BW1308 and BW1517-BW1521), with D_{Cd} values ranging from 0.26 to 3.7 (Table 1, Fig. 2).

The graphite capsule time-series experiments (BW1517-BW1521) were carried out to identify the time taken for an experiment to reach chemical and isotopic equilibrium with regards to Cd metal-silicate exchange. The Cd concentrations range from 3251 to 4911 μg/g in the silicate phases of these experiments, and from 1265 to 3507 μg/g in the metal. Of these five experiments, BW1521 and BW1518 were the shortest, with durations of 4 and 12 min, respectively, and they display the highest D_{Cd} values of 1.1 ± 0.3 and 0.82 ± 0.16 (2SD). The D_{Cd} values for the remaining three time-series experiments, which lasted 30 min or more, are similar, with an average D_{Cd} of 0.41 ± 0.27 (2SD) (Table 1, Fig. 2). Only the results of the latter experiments are discussed in the following because the experimental times are consistent with those previously shown to be appropriate for attainment of equilibrium in the applied capsules by Tuff et al. (2011).

Experiments BW1305 to BW1308 were carried out in different capsule materials at variable temperatures with durations exceeding 56 min. Cadmium exhibited weakly siderophile behaviour in these experiments, with D_{Cd} values ranging from 1.7 to 3.7. Specifically, the experiments conducted in silica (BW1305) and MgO (BW1307) capsules are characterised by D_{Cd} values of 1.8 ± 0.1 and 3.5 ± 0.7 (2SD), respectively. The graphite capsule experiments BW1306 and BW1308, which utilised different starting compositions and run temperatures, define roughly similar D_{Cd} values of 1.7 ± 0.1 and 3.7 ± 0.3 (2SD), respectively (Table 1, Fig. 2).

Major element analyses of the silicate phases from the two graphite capsule experiments (BW1306 and BW1308) generally reflect the starting compositions of the silicate fractions, with additional Fe derived from the metal component (Table S1, Supplementary material). The Cd concentrations of the graphite capsule metal phases are 11,416 and 12,018 μg/g, and 3283 and 6605 μg/g for the silicate phases. In comparison, the MgO capsule metal and silicate phases have considerably lower Cd concentrations of 164 and 47 μg/g, respectively. Similarly, the metal and silicate products from the silica capsule runs have Cd concentrations of 33 and 18 μg/g, considerably lower than those of the CMAS starting material (0.4 to 1% wt%), and the metal and silicates from the graphite capsule experiments. This indicates that more than about 98% of the added Cd was lost during the MgO and silica capsule experiments, whilst less than about 10% of Cd was lost from the graphite

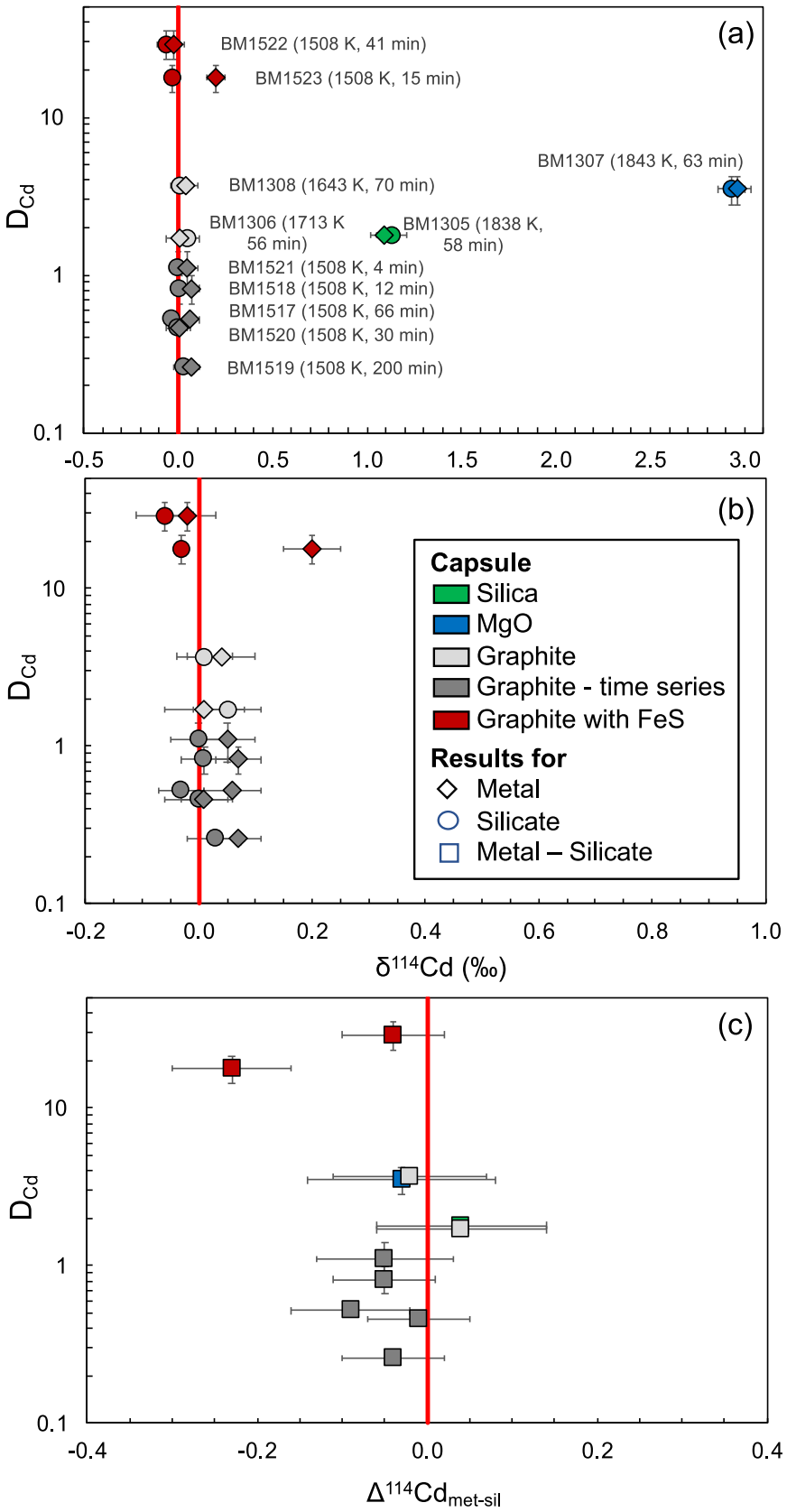

Fig. 2. Panels (a) and (b) show plots of D_{Cd} versus $\delta^{114}Cd$ for the metal and silicate phases of the partitioning experiments. Panel (c) shows a plot of D_{Cd} versus the metal-silicate isotope fractionation factors $\Delta^{114}Cd_{met\text{-}sil}$ for the same experiments.

capsules.

The D_{Cd} values for the Fe sulphide-silicate partitioning experiments BW1522 and BW1523 are 29.1 ± 5.8 and 17.9 ± 3.6 (2SD) respectively, with experiment BW1522 lasting longer than BW1523 (41 versus 15 min, respectively). Compared to experiment BW1523, the silicate and sulphide phases of BW1522 have higher Cd concentrations, of 221 versus 144 μg/g and 6441 versus 2582 μg/g, respectively, most likely due to Cd loss during the former experiment (Table 1, Fig. 2).

4.1.2. Cadmium metal-silicate isotope fractionation

The Cd isotope compositions of the silicate, metal and sulphide phases from all experiments are either heavier or within error of the Cd-doped CMAS starting material (Table 1, Fig. 2). Metal and silicate products from the MgO capsule experiment BW1307 display significantly heavier Cd isotope compositions than the starting materials, with δ^{114}Cd values of +2.93 ± 0.07‰ and + 2.96 ± 0.08‰ (2SE), respectively. Similarly, the metal and silicate phases from the silica capsule experiment BW1305 have δ^{114}Cd values of +1.13 ± 0.07‰ and + 1.09 ± 0.08‰ (2SE), respectively (Table 1; Fig. 2). These heavy Cd isotope enrichments are coupled with significant Cd loss during the MgO and silica experiments.

The degree of Cd isotope fractionation during metal-silicate separation is given by the difference between the Cd isotope compositions of the metal (or sulphide), and silicate phases:

$$\Delta^{114}Cd_{met-sil} = \delta^{114}Cd_{met} - \delta^{114}Cd_{sil} \quad (3)$$

Whilst the majority of the experiments have slightly negative $\Delta^{114}Cd_{met\text{-}sil}$ values, the average $\Delta^{114}Cd_{met\text{-}sil}$ calculated from all metal-silicate experiments (bar the short duration experiments BW1521 and BW1518) is −0.02 ± 0.09‰ (2SD; $n = 7$). Hence, there is no significant Cd isotope fractionation between metal and silicate even in experiments which have manifestly lost Cd. Furthermore, there is no systematic relationship between $\Delta^{114}Cd_{met\text{-}sil}$ and temperature, run duration, capsule material or the extent of Cd loss (Table 1; Fig. 2).

Whilst experiment BW1522 also shows no significant isotope fractionation between sulphide and silicate ($\Delta^{114}Cd_{sul\text{-}sil} = -0.04 \pm 0.06$‰; 2SE), BW1523 displays the largest isotope fractionation observed in this study, with a $\Delta^{114}Cd_{sul\text{-}sil}$ value of −0.23 ± 0.07‰ (2SE).

5. Discussion

5.1. Insights from Cd metal-silicate partitioning experiment

5.1.1. Kinetic Cd isotope fractionation and volatilisation

Metal and silicate phases from the MgO and silica capsule experiments display substantial loss of Cd and the greatest enrichment in heavy Cd isotopes relative to the starting CMAS composition (Fig. 2, Table 1). Whilst melt dilution due to dissolution of capsule wall material may have lowered Cd concentrations in the experimental products of runs BW1305 (SiO_2 capsule) and BW1307 (MgO capsule) to some extent, the significant Cd depletions, with more than about 98% of added Cd lost, most likely reflect volatilisation and loss of Cd, coupled with attenuated kinetic isotope fractionation from a partially open system. Volatilisation thereby produced vapour enriched in light Cd isotopes, which escaped the system. Although the silica capsule run products display a larger degree of Cd depletion, those from the MgO experiment have the heaviest Cd isotope compositions, suggesting the MgO experiment experienced a greater degree of Cd loss. This may reflects increased silicate melt volume in experiment BW1305 by the dissolution of the silica capsule, a mechanism previously proposed by Bridgestock et al. (2014) to explain the same phenomena in their Zn partitioning experiments. Alternatively, the isotopic differences may record different effective isotope fractionation factors, due to variable attenuation of kinetic isotope fractionation by different extents of back-reaction.

Despite the large observed differences in the extent of Cd loss from the different experiments, the calculated metal-silicate isotope fractionations $\Delta^{114}Cd_{met\text{-}sil}$ agree with one another within uncertainty (Fig. 2; Table 1). This indicates that the metal ball and surrounding silicate liquid rapidly exchanged Cd whilst Cd loss was occurring during the experiments (Fig. 1).

5.1.2. Effects of temperature and composition on cadmium metal-silicate partitioning

The D_{Cd} values determined from the three graphite capsule time-series experiments with a duration of 30 min to 200 min are very similar to one another, with results of between 0.52 and 0.26. These D_{Cd} data broadly resemble the results of Lagos et al. (2008) but they are lower than the D_{Cd} values of 1.7 and 3.7 obtained in the graphite capsule experiments BW1306 and BW1308 (Fig. 2, Table 1). Relative to the latter, the silica and MgO capsule experiments BW1305 and BW1307 yielded similar D_{Cd} results of 1.8 and 3.5. The experiments BW1305 to BW1308 were carried out at the highest temperatures (of >1640 K) and BW1305 to BW1307 utilised the same starting materials. In contrast, all time-series experiments (BW1517 to BW1521) were run at a lower temperature of about 1500 K. They and experiment BW1308 featured a silicate starting composition containing about 50 to 60 wt% $Na_2Si_2O_5$ (Fig. 2, Table 1).

At first glance, the data for all seven metal-silicate experiments with a duration of ≥30 min could suggest that Cd becomes more siderophile with increasing temperature, consistent with the work of Ballhaus et al. (2013). To assess the controls on D_{Cd}, multiple linear regression analyses were carried out, combining data from this and previous studies (Fig. 3, Supplementary Fig. S1). The results of these analyses show that temperature has no statistically significant effect on D_{Cd}. Given this, the small observed differences in D_{Cd} most likely primarily reflect different extents of carbon dissolution into the metal during the graphite capsule experiments. Lagos et al. (2008) measured 5 to 7 wt% carbon for the metal phases of their graphite capsule experiments, presumably from graphite dissolution, whilst Marin et al. (2013) reported depressed D_{Cd} values for graphite capsule experiments relative to those in MgO capsules. The results of our multiple linear regression analyses (see below) further support these findings, as higher C concentrations in the metal are associated with decreasing D_{Cd}.

The D_{Cd} values for the Fe sulphide-silicate partitioning experiments BW1522 and BW1523 are much higher (29.1 ± 5.8 and 17.9 ± 3.6) than those of the metal-silicate experiments. The results are furthermore in accord with previous findings (Lagos et al., 2008; Wood et al., 2014; Steenstra et al., 2017; Kubik et al., 2021), which show that D_{Cd} increases significantly as the S content of the metal phase increases.

5.1.3. Multiple linear regression for Cd metal-silicate partitioning

The metal-silicate partitioning of Cd is related to the metal-silicate exchange coefficient (K_D) for Cd and Fe, with K_D given by:

$$K_D(Cd) = D_{Cd}^{met/sil} \Big/ D_{Fe}^{met/sil} \quad (4)$$

and where D_{Cd} and D_{Fe} represent the metal-silicate partition coefficients of Cd and Fe, respectively. Following Righter (2011), the following expression can be used to fit K_D:

$$lnK_D = \frac{a}{T} + \frac{bP}{T} + cln(1 - X_S) + dln(1 - X_C) + eln(1 - X_{Si}) + f(nbo/t) + g \quad (5)$$

Here, T is temperature (K), P is pressure (GPa), X_S, X_C and X_{Si} are the molar fractions of S, C, and Si in the metal phase, nbo/t is the degree of silicate polymerisation, and a to g are best-fit constants.

Least squares multiple linear regression (MLR) analyses were carried out to constrain the values of coefficients a to g based on data from 207 Cd partitioning experiments from this study and the literature (Lagos et al., 2008; Ballhaus et al., 2013; Wood et al., 2014; Wang et al., 2016;

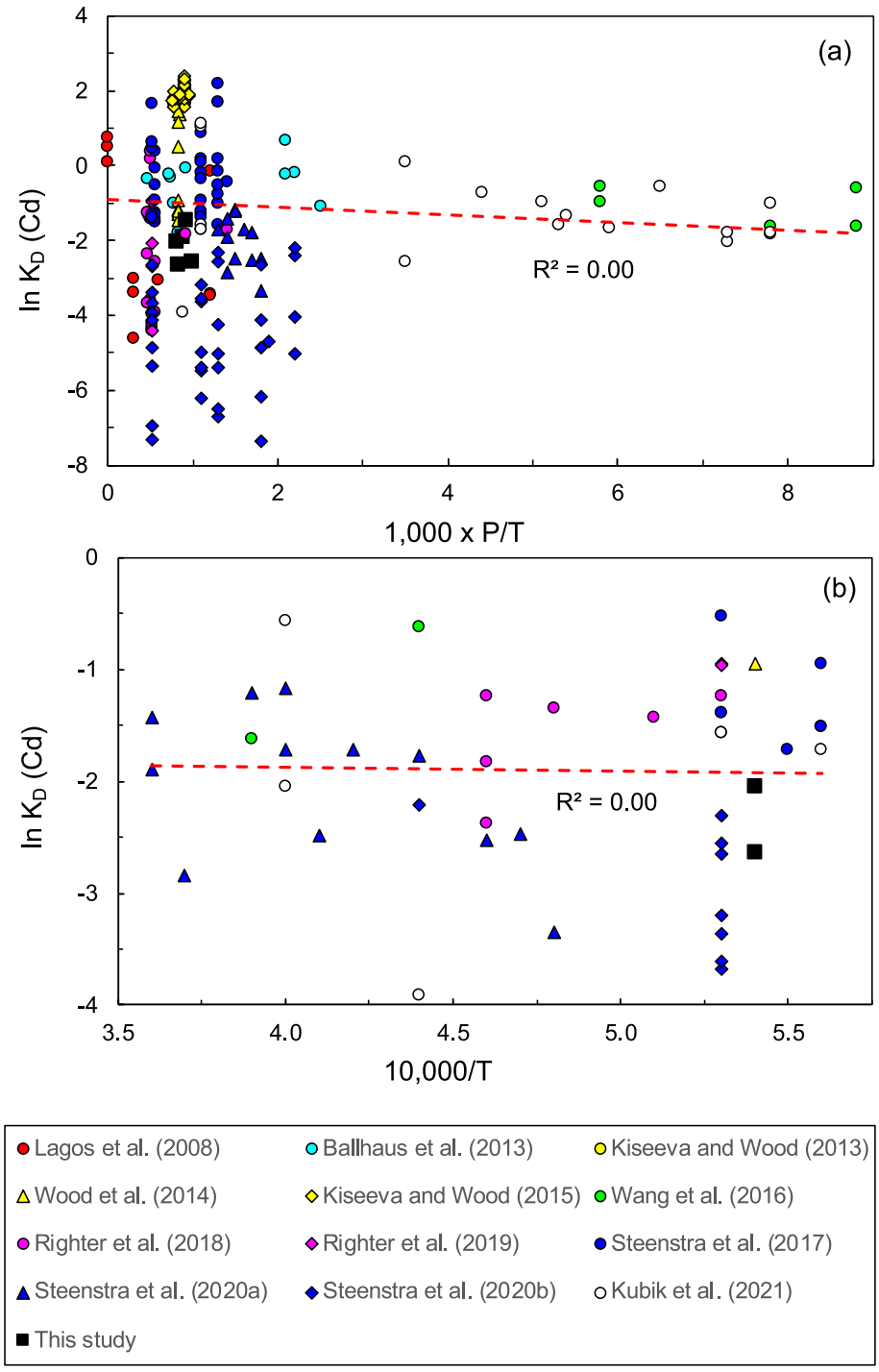

Fig. 3. Plot of ln K_D values for Cd versus (a) 1000 x P/T and (b) 10,000/T for experimental data from this study (Table 1) and previous investigations (Supplementary Material, Table S2). Only data for experiments that are free of S, C and Si (with $\ln(1 - X_{S/C/Si}) \geq -0.01$) are plotted in panel (b).

Steenstra et al., 2017; Righter et al., 2018; Righter et al., 2019; Steenstra et al., 2020b; Steenstra et al., 2020a; Kubik et al., 2021). All data used in the MLR analyses are summarised in Table S2, whilst Fig. S1 summarises how K_D varies as a function of the variables of Eq. (5) (see Supplementary material). The method of Mills et al. (2014) was used to estimate nbo/t for each experiment, with all Fe assumed to be in the form of FeO for simplicity. The independent variables outlined in Eq. (5) were considered statistically significant if a *p*-value of <0.05 was obtained from an MLR analysis.

An initial MLR analysis showed that P/T had no statistically significant impact on ln K_D, with $p = 0.25$ and an R^2 value of 0 (Fig. 3a), and so it was disregarded in subsequent analyses. Whilst the analyses also suggested that both 1/T and nbo/t are significant predictors of ln K_D, there was a significant level of multicollinearity between the two variables ($R^2 = 0.56$). Multicollinearity can render models less robust and introduce significant artefacts and therefore needs to be carefully considered. Thus, two further MLR analyses were carried out to assess the predicting power of 1/T and nbo/t. The first of these analyses included nbo/t, ln (1-X_S), ln (1-X_C), and ln (1-X_{Si}) and this revealed that nbo/t is not a statistically significant predictor of ln K_D (Fig. S1, Supplementary material), with a p-value of 0.28. The second included 1/T, ln (1-X_S), ln (1-X_C), and ln (1-X_{Si}), and suggested that temperature has a

significant effect on K_D ($p < 0.01$; Fig. S1, Supplementary material). However, minor levels of multicollinearity were also found between ln (1-X_S) and 1/T ($R^2 = 0.24$). Therefore, the predicting power of temperature was further tested through regression analysis of 46 experiments free of S, C, and Si (specifically with $\ln(1\text{-}X_{S/C/Si}) \geq -0.01$). This analysis (Fig. 3b) showed that temperature has no statistically significant impact on ln K_D ($p = 0.86$, $R^2 = 0$) and 1/T was hence also excluded from further consideration. This does not preclude that 1/T has an impact on ln K_D but suggests that the impact is most likely minor and hence lost in the scatter of data that were obtained in experiments with different compositions and in various laboratories. The final MLR analyses were, therefore, focussed on ln (1-X_S), ln (1-X_C), and ln (1-X_{Si}) (Fig. S1, Supplementary material), and gave the following predictive expression for ln K_D, with an adjusted R^2 value of 0.80 (2SE coefficient uncertainties are also shown):

$$ln K_D = -5.5 \pm 0.6 \bullet ln(1 - X_S) + 6.9 \pm 2.2 \bullet ln(1 - X_C) + 21 \pm 2 \bullet ln(1 - X_{Si}) - 1.6 \pm 0.2 \quad (6)$$

These findings are broadly consistent with the multiple linear regression of Kubik et al. (2021), who found that metal-silicate partitioning of Cd is independent of both temperature and pressure, Furthermore, the current study and the investigations of Kubik et al. (2021) and Wood et al. (2014) predict similar increases of K_D(Cd), and hence D_{Cd}, for increasing S contents of the metal. For example, for a metal sulphide with $X_S = 0.4$, the formalisms of this study, Kubik et al. (2021) and Wood et al. (2014) yield identical K_D(Cd) values of 3.8 ± 1.8, 2.5 ± 1.4 and 1.9 ± 0.5, respectively. Novel to the current study is that the presented regression also shows that the presence of C and Si in the metal cause Cd to act in a more lithophile manner during metal-silicate equilibration.

5.1.4. Cadmium isotope fractionation during metal-silicate partitioning

No systematic relationship was found between $\Delta^{114}Cd_{met\text{-}sil}$ and temperature, experiment duration, or capsule material, and no significant Cd isotope fractionation between metal and silicate was observed, as the experiments, excluding the short runs BW1521 and BW1518, define a mean $\Delta^{114}Cd_{met\text{-}sil} = -0.02 \pm 0.09$‰ (2SD; $n = 7$). Of interest is the observation that the results obtained with MgO and silica capsules are identical to those from graphite capsules, even though the former experimental products lost considerable Cd by volatilisation with significant associated kinetic Cd isotope fractionation (Fig. 2, Table 1). This observation demonstrates that the Cd remaining in the capsules exchanged rapidly between metal and silicate, thus providing a mechanism by which the isotopic equilibrium between the phases could be established and maintained. This conclusion is in accord with the findings of previous partitioning experiments that were conducted in capsules similar to those utilised in the present study (Wood et al., 2008; Tuff et al., 2011; Bridgestock et al., 2014).

Both laboratory experiments (Guinoiseau et al., 2018) and observations from naturally occurring hydrothermal settings (Schmitt et al., 2009; Xie et al., 2019) show that sulphide phases preferentially incorporate light Cd isotopes during precipitation at lower temperatures. Despite this, no resolvable Cd isotope fractionation was observed between the silicate and sulphide phases of experiment BW1522. The sulphide phase of experiment BW1523 displays a lighter Cd isotope composition than the silicate but this experiment was shorter than BW1522 (at 15 min compared to 41 min) and the phases show clear evidence of Cd loss relative to BW1522 (Table 1). During the sulphide-silicate experiments, Cd was much more concentrated in the sulphide phase (due to $D_{sul\text{-}sil} \geq 17.9$; Table 1) than in the metal of the metal-silicate partitioning experiments. As such, the results for BW1523 may reflect that isotopic equilibrium could not be fully maintained during volatile loss, as Cd was primarily concentrated in only one of the phases.

Through a series of similar experiments, Bridgestock et al. (2014) found there was no significant Zn isotope fractionation between metal and silicate phases, while Mahan et al. (2017) observed no relationship between Zn isotope fractionation and temperature, composition or oxygen fugacity. Given the chemical similarities of Zn and Cd, it is perhaps not surprising that they share an absence of isotope fractionation during metal-silicate partitioning. These findings suggest that no or only very minor Cd isotope fractionation occurred during core segregation on Earth. Whilst metal segregation during Earth's core formation took place at higher temperature and pressure than those attained in the experiments, higher temperatures should only reduce equilibrium isotope fractionation factors whilst changes in pressures are not expected to have a significant impact on the extent of isotope fractionation (O'Neil, 1986).

5.2. Modelling Earth's Cd budget during accretion and differentiation

Chou (1978) argued that the addition of a small late veneer of chondritic material, equivalent to about 1% of BSE mass, after cessation of core formation could explain the roughly chondritic platinum group element ratios inferred for the silicate Earth from analyses of ultramafic rocks. Since then, numerous elemental and isotopic studies concluded that Earth likely received a late veneer of chondritic origin once core formation was complete (Wänke, 1981; Meisel et al., 1996; Meisel et al., 2001; Wang and Becker, 2013; Laurenz et al., 2016; Young et al., 2016; Fischer-Gödde and Kleine, 2017; Varas-Reus et al., 2019; Fischer-Gödde et al., 2020; Hopp et al., 2020; Hellmann et al., 2021). It is unresolved, however, whether this late veneer is of carbonaceous, enstatite or ordinary chondrite origin and its mass is also debated. Based on mantle HSE abundances, the late veneer mass is most commonly estimated at about 0.5% M_E but other workers have posited that a much larger volatile-rich late veneer of between 2% and 5% M_E contributed the bulk of the BSE inventory of volatile elements (e.g., Holzheid et al., 2000; Walker, 2009; Albarède, 2009; Ballhaus et al., 2013; Laurenz et al., 2016; Jacobson et al., 2014).

The accretion and core formation model presented in the following integrates available constraints on the elemental and isotopic partitioning of Cd with reasonable endmember estimates for the mass and composition of the late veneer, in order to assess the composition of Earth's main stage accretion material. The model is developed in two main stages. The first stage describes single-stage core formation as a batch process alongside accretion, whilst the second stage involves the addition of a chondritic late veneer. Given constraints on the composition of the late veneer, mass balance modelling is first carried out to estimate the Cd isotope composition of the BSE prior to delivery of the late veneer. This composition is then used with core formation calculations to derive the mean Cd concentration and isotope composition of Earth's main stage accretion components and assess previous estimates of late veneer mass. Model inputs are summarised in Table 2 and discussed in the following. To account for uncertainties in the input parameters, the modelling utilised a Monte Carlo approach, whereby a uniform distribution was used to randomly select a given value for each iteration of the model. The uncertainties of the model outputs (Table 3, Figs. 3, 4) encompass the full range of results that are in accord with the model constraints.

5.2.1. Modelling the impact of the late veneer on the silicate Earth Cd budget

The first part of the model uses an inverse mass balance approach to constrain the Cd concentration and isotope composition of the initial BSE after the cessation of core formation, but before arrival of the late veneer. The Cd concentration of the BSE can be represented by the following expression:

$$[Cd]_{BSE} = \left([Cd]_{LV} \times F_{LV}\right) + \left([Cd]_{i-BSE} \times (1 - F_{LV})\right) \quad (7)$$

where $[Cd]_{LV}$ is the Cd concentration of the late veneer, $[Cd]_{i\text{-}BSE}$ is the Cd concentration of the initial pre-late veneer BSE after core formation

Table 2
Input parameters for the terrestrial Cd accretion models.

		Source
Cd abundances (ng/g)		
Present-day BSE	38 ± 6	a
Late veneer	700 (CI, EH); 40 (CO, EL)	b
Cd isotope compositions		
δ^{114}Cd BSE	−0.06 ± 0.06	c
δ^{114}Cd Late veneer	0.34 ± 0.12	d
Core segregation		
$D_{Cd\ (met\text{-}sil)}$ (lower limit)	0.4	e
$D_{Cd\ (met\text{-}sil)}$ (upper limit)	8	e
$\Delta^{114}Cd_{met\text{-}sil}$	0.00 ± 0.05	e
Hadean matte segregation		
Mass fraction of Hadean matte	0.8% of BSE	f
$D_{Cd\ (sul\text{-}sil)}$	33	g
$\Delta^{114}Cd_{sul\text{-}sil}$	−0.18 ± 0.04	h

(a) Wang et al. (2018). (b) Based on CI and EH chondrite data of Wasson and Kallemeyn (1988), Lodders and Fegley (1998), Palk et al. (2018), Braukmüller et al. (2018). (c) Pickard et al. (2022). (d) Based on Cd isotope compositions of CI and EH chondrites from Baker et al. (2010) and Palk et al. (2018). (e) This study; see text for details. (f) Savage et al. (2015). (g) A Hadean matte (HM) with 46 ± 16 wt% Fe and X_S = 0.43 ± 0.09 (O'Neill, 1991) was generated by combining the stoichiometric Fe-S-O HM mixture of Savage et al. (2015) with the mantle sulphide composition of Lorand and Conquéré (1983). The sulphide-silicate D_{Cd} associated with the HM was determined by using Eq. (6) with a HM X_S = 0.43 ± 0.09 and assuming a sulphide-silicate D_{Fe} = 7.3, calculated by combining the mantle Fe estimate of Wang et al. (2018) with the HM estimate of 46 ± 16 wt% Fe. (h) This study; see text for details. A maximum $\Delta^{114}Cd_{sul\text{-}sil}$ value was estimated by considering the effect of S on experiment BW1523 relative to the S-free experiments and extrapolating to X_S = 0.43 ± 0.09 for the HM.

had ceased, and F_{LV} is the mass fraction of the modern BSE derived from the late veneer. The Cd concentration of the BSE is well defined as 38 ± 6 ng/g by Wang et al. (2018), who evaluated previous $[Cd]_{BSE}$ estimates that are based primarily on peridotite analyses (Table 2). Given the uncertainties about the heritage of the late veneer and hence its Cd concentration, two endmember compositions are evaluated in the following for $[Cd]_{LV}$. The first assumes that $[Cd]_{LV}$ matches the Cd concentrations of volatile-rich CI carbonaceous and EH enstatite chondrites, with approximately 700 ng/g Cd. In contrast, the second is significantly less volatile-rich with $[Cd]_{LV}$ = 40 ng/g, similar to the Cd abundances of CO carbonaceous, EL enstatite as well as ordinary chondrites (OCs; Table 2). With these constraints, the Cd concentration of the i-BSE prior to delivery of the late veneer can be determined as a function of late veneer mass using Eq. (7).

In a similar manner, the Cd isotope composition of the BSE is represented by the equation:

$$\delta^{114}Cd_{BSE} = \left(\delta^{114}Cd_{LV} \times f_{Cd}\right) + \left(\delta^{114}Cd_{i-BSE} \times (1 - f_{Cd})\right) \quad (8)$$

where $\delta^{114}Cd_{LV}$ is the Cd isotope composition of the late veneer, $\delta^{114}Cd_{i\text{-}BSE}$ is the initial Cd isotope composition of the BSE as core formation ceased, and f_{Cd} is the fraction of Cd in the BSE derived from the late veneer. Eq. (8) can thus be used to derive $\delta^{114}Cd_{i\text{-}BSE}$ as a function of late veneer mass, whereby the Cd isotope compositions of the BSE and the late veneer are boundary conditions. Based on analyses of spinel lherzolites, Pickard et al. (2022) inferred a BSE composition of $\delta^{114}Cd_{BSE}$ = −0.06 ± 0.03‰ but an expanded uncertainty of ±0.06‰ is employed in the following to account for the small number of samples that were analysed to determine the mean (Table 2).

Constraining $\delta^{114}Cd_{LV}$ is more challenging because the origin of the material is unclear, with carbonaceous, enstatite and ordinary chondrites suggested as possible late veneer sources (Meisel et al., 1996; Meisel et al., 2001; Wang and Becker, 2013; Laurenz et al., 2016; Young et al., 2016; Dauphas, 2017; Varas-Reus et al., 2019; Fischer-Gödde et al., 2020; Hellmann et al., 2021), and only limited data are available for such meteorites. Particularly scarce are δ^{114}Cd data that are precise to about ±0.1‰ as these are currently only available for seven carbonaceous chondrites (CI, CM, CV, CO, CR) as well as eight EH and EL enstatite chondrites (Baker et al., 2010; Palk et al., 2018; Supplementary Table S3). Of these, four carbonaceous chondrites and two EH chondrites have high Cd concentrations (≥ 95 ng/g) and δ^{114}Cd values of between about +0.22 and + 0.46‰, which likely approximate the isotope compositions of the parent bodies. The remaining samples, typically with Cd abundances of <40 ng/g, have higher δ^{114}Cd of up to about 7‰. These heavy Cd isotope compositions are most likely due to Cd redistribution by thermal and shock metamorphism on the parent

Table 3
Results of mass balance model for Cd during Earth's accretion as a function of late veneer mass.

Late veneer mass (% M_E)	0.5%	1%	2%	3%
CI-EH late veneer				
*Cd BSE budget from late veneer**	14 ± 2%	29 ± 5%	56 ± 9%	85 ± 14%
Main stage accretion material – Standard model				
Cd abundance (ng/g), D_{Cd} = 0.4	26 ± 5	22 ± 5	14 ± 5	6 ± 5
Cd abundance (ng/g), D_{Cd} = 8	110 ± 20	94 ± 20	60 ± 21	24 ± 21
δ^{114}Cd	−0.12 ± 0.13	−0.25 ± 0.18	−0.69 ± 0.50	−13.9 ± 13.3
Main stage accretion material – Hadean matte model				
Cd abundance (ng/g), D_{Cd} = 0.4	33 ± 6	28 ± 6	18 ± 7	7 ± 6
Cd abundance (ng/g), D_{Cd} = 8	136 ± 25	116 ± 25	74 ± 26	30 ± 27
δ^{114}Cd	−0.17 ± 0.12	−0.28 ± 0.18	−0.74 ± 0.50	−14.2 ± 13.6
Bulk Earth composition – both models				
Cd abundance (ng/g), D_{Cd} = 0.4	34 ± 9	32 ± 8	30 ± 7	28 ± 6
Cd abundance (ng/g), D_{Cd} = 8	128 ± 36	113 ± 34	82 ± 30	49 ± 26
δ^{114}Cd	−0.13 ± 0.13	−0.20 ± 0.18	−0.43 ± 0.41	−1.42 ± 1.38
CO-EL late veneer				
*Cd BSE budget from late veneer**	0.8 ± 0.1%	1.6 ± 0.3%	3.2 ± 0.5%	4.9 ± 0.8%
Main stage accretion material – Standard model				
Cd abundance (ng/g), D_{Cd} = 0.4	30 ± 5	30 ± 5	30 ± 5	30 ± 5
Cd abundance (ng/g), D_{Cd} = 8	126 ± 20	127 ± 20	128 ± 21	130 ± 22
δ^{114}Cd	−0.06 ± 0.08	−0.07 ± 0.10	−0.07 ± 0.10	−0.08 ± 0.10

The average Cd concentrations and δ^{114}Cd values of Earth's main stage accretion material and bulk Earth compositions were determined by Monte Carlo simulations with model inputs summarised in Table 2. For the CO-EL late veneer models, the bulk Earth compositions are not given as these closely resemble the compositions of the main stage accretion material (to within 2% for Cd concentrations and to within 0.02‰ for δ^{114}Cd). The quoted uncertainties encompass the full range of results that were obtained in the modelling as a consequence of variable input parameters ($\delta^{114}Cd_{BSE}$, $\Delta^{114}Cd_{met\text{-}sil}$, $\Delta^{114}Cd_{sul\text{-}sil}$) and for BSE Cd concentrations of 38 ± 6 ng/g. The total uncertainties are primarily governed by the uncertainty of the latter parameter. * Mass fraction of the BSE Cd inventory derived from the late veneer in %.

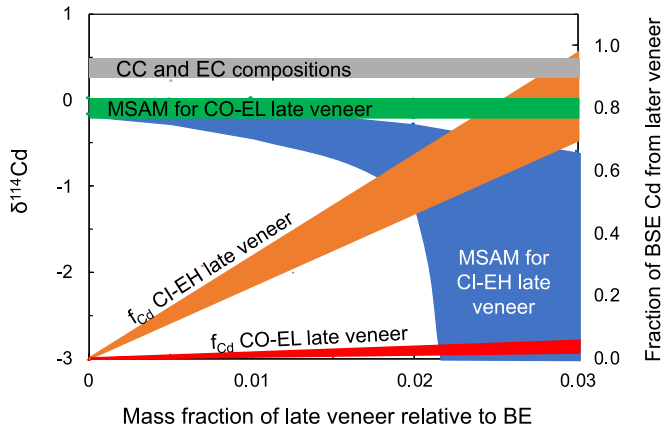

Fig. 4. Plot that summarises results of terrestrial accretion models for Cd. The blue and green fields show the range of δ^{114}Cd values (including uncertainties) required for Earth's main stage accretion material (MSAM) to reproduce the Cd isotope composition of the BSE, as a function of late veneer mass, for a late veneer composed either of volatile-rich CI-EH or volatile-poor CO-EL material. The orange and red fields denote the mass fraction of BSE Cd (f_{Cd}) derived from either a CI-EH or CO-EL late veneer, also as a function of late veneer mass. Model inputs and results are outlined in Tables 2 and 3, respectively. The grey field represents the range of Cd isotope compositions previously measured for carbonaceous and enstatite chondrites (CC, EC) that are thought to be unaffected by Cd redistribution during metamorphism (Baker et al., 2010; Palk et al., 2018). (For interpretation of the references to colour in this figure legend, the reader is referred to the web version of this article.)

bodies and are therefore unlikely to be representative of the bulk asteroids (Wombacher et al., 2003; Wombacher et al., 2008). Additional data, from older analyses with larger δ^{114}Cd uncertainties of between about ±0.45‰ to ±1‰, are available for ordinary chondrites and eucrites as well as samples from Moon and Mars (Wombacher et al., 2003; Wombacher et al., 2008). These analyses provide highly variable δ^{114}Cd values of between about −9‰ and 15‰ for the ordinary chondrites that are thought to reflect parent body processes that involve mobilisation of Cd. As such, no robust estimates of parent body compositions are possible for the ordinary chondrites. Similar isotopic variability was reported for two lunar meteorites, a pristine ferroan anorthosite and lunar soils, which exhibit δ^{114}Cd values of about 1‰ to 11‰ (Wombacher et al., 2008). In contrast, analyses of two shergotites and two eucrites yielded δ^{114}Cd of between about 0‰ and 1‰, which suggests that the silicate portions of Vesta and Mars may have compositions similar to the BSE with δ^{114}Cd ≈ 0‰. Considering the available results for meteorites, and particularly the more precise data published for carbonaceous and EH chondrites where the Cd systematics are most likely unaffected by parent body processes, a $\delta^{114}Cd_{LV}$ value of 0.34 ± 0.12‰ is employed in the following to approximate the composition of the chondritic late veneer (Table 2).

5.2.2. Modelling the impact of core formation on the silicate Earth Cd budget

The second part of the accretion model describes Earth's growth and core formation. Continuous core formation models account for changes in metal-silicate partitioning associated with increasing temperature and pressure of Earth's interior during accretion, as well as changes in oxygen fugacity and volatile element abundances associated with heterogeneous accretion. Problems arise, however, when such continuous models are employed to predict Cd partitioning. Firstly, Cd metal-silicate partitioning is primarily dependent on the abundances of S, C and Si in the Earth's core and estimates of these concentrations throughout accretion involve significant uncertainty. Secondly, both S and C are volatile elements. As the overarching aim of the study is to evaluate the delivery of terrestrial volatiles, it is inappropriate to assess the accretion history of Cd by assuming the S and C contents of the core through time, and by inference, the accretion history of volatiles. Lastly, initial modelling carried out for this study showed that, taking into account uncertainties in the bulk Earth composition, single-stage accretion models yielded similar results to models that employed continuous core formation and in which reasonable changes in mantle oxygen fugacity and a range of X_S, X_C, and X_{Si} values were considered. Notably, this reflects the insensitivity of the partitioning of Cd (and its isotopes) to changes in temperature and pressure (Fig. 3) and the weak siderophile character of Cd, whereby its BSE signature integrates over most of the accretion process (Dauphas, 2017). As such, a single-stage core formation model is applied in the following.

Assuming single-stage core formation, Eq. (6) can be combined with estimates for the X_S, X_C, and X_{Si} values of Earth's core, to determine an effective K_D for the Earth's core-mantle system. The X_S (0.0268 ± 0.0069), X_C (0.0309 ± 0.0267) and X_{Si} (0.0829 ± 0.0396) values of the core were calculated from the concordance core composition of Wang et al. (2018). This gives a ln K_D value of −3.5 ± 1.8 (2SE), which corresponds to a D_{Cd} of 0.39, assuming a core-mantle D_{Fe} of 13.1. The inferred D_{Cd} value, however, stands in contrast to the high Cd concentration that was estimated for the bulk Earth by Braukmüller et al. (2019) and which indicates that Cd is enriched in the core relative to the BSE by a factor of about 5 to 10. Furthermore, recent accretion modelling and multiple linear regression analyses of metal-silicate partitioning data by Kubik et al. (2021) suggest that Cd is siderophile with a final D_{Cd} of between about 1 and 8 for the core-mantle system. The higher D_{Cd} obtained by Kubik et al. (2021) likely reflects that their data analysis did not account for C and Si present in the metal, two elements that reduce the siderophile nature of Cd. Given current uncertainties about the light element composition of Earth's core, two endmember models were examined, which assume D_{Cd} values of 0.4 and 8 to describe core-mantle partitioning (Tables 2, 3).

Core formation was then modelled as a batch process using the following equation:

$$[Cd]_{i-BSE} = \frac{[Cd]_{MSAM}}{F_{i-BSE} + D_{Cd}(1 - F_{i-BSE})} \quad (9)$$

where $[Cd]_{MSAM}$ is the mean Cd concentration of Earth's main stage accretion material, and$F_{i\text{-}BSE}$ is the mass fraction of the initial BSE after core formation relative to the pre-late veneer bulk Earth. Core formation and associated Cd partitioning can be accompanied by isotope fractionation, described by the equation:

$$\delta^{114}Cd_{i-BSE} = \delta^{114}Cd_{MSAM} - \left(\Delta^{114}Cd_{met-sil} \times (1 - f_{i-Cd})\right) \quad (10)$$

where $\delta^{114}Cd_{MSAM}$ is the mean Cd isotope composition of Earth's main stage accretion material, $f_{i\text{-}Cd}$ is the fraction of Cd present in the silicate mantle after core formation, and $\Delta^{114}Cd_{met\text{-}sil}$ is the Cd isotope fractionation between the core and BSE. A value of 0.00 ± 0.05‰ was chosen for the Cd isotope fractionation during core formation, in accord with the absence of significant isotope fractionation in the experiments of this study (Table 1). As both $[Cd]_{i\text{-}BSE}$ and $\delta^{114}Cd_{i\text{-}BSE}$ are derived from the late veneer mass balance calculations, it is possible to constrain the average Cd concentration and isotope composition of Earth's main stage accretion material, as a function of late veneer mass.

5.2.3. Results of accretion modelling for Cd

Model inputs and results are outlined in Tables 2 and 3 as well as Figs. 4 and 5. If a volatile-rich CI- or EH-like composition is assumed for the late veneer, in accord with previous studies, the addition of this material has a significant impact on the Cd inventory of the BSE even if the late veneer mass is small (Meisel et al., 1996; Meisel et al., 2001; Laurenz et al., 2016; Varas-Reus et al., 2019). For example, a CI-EH late veneer of 0.5% M_E still provides 14 ± 2% of the BSE Cd budget and this proportion rises to 85 ± 14% for a late veneer mass of 3% M_E (Fig. 4, Table 3). For a BSE with 38 ± 6 ng/g Cd, the mass balance calculations

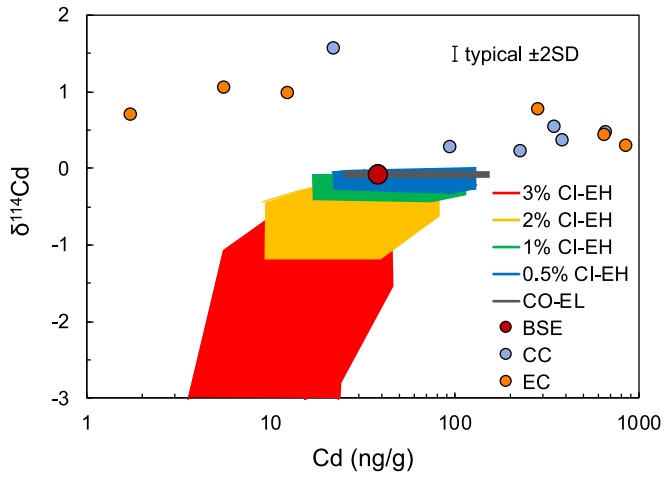

Fig. 5. Cd isotope compositions and concentrations of Earth's main stage accretion material, as predicted by accretion modelling, with results outlined in Table 3. The fields denote the Cd concentrations and isotope compositions (including uncertainties; Table. 3) predicted for Earth's main stage accretion material for 0.5% to 3% M_E addition of either a volatile-rich CI-EH late veneer (blue, green, orange, red fields) or a volatile-depleted CO-OC late veneer (single grey field). The range of Cd concentrations and δ^{114}Cd values reflect a BSE with 38 ± 6 ng/g Cd and D_{Cd} values that range from 0.4 to 8 for single-stage core-mantle partitioning (see text and Table 2 for details). Also shown are the composition of the BSE (Table 2) and precise literature Cd isotope data for carbonaceous chondrites (CC) and enstatite chondrites (EC) from Baker et al. (2010) and Palk et al. (2018). (For interpretation of the references to colour in this figure legend, the reader is referred to the web version of this article.)

provide an upper limit of about 3.1 to 4.2% M_E for the late veneer mass, as any further increase would supply more Cd than is present in the BSE. This value increases to about 6 to 8% M_E if a less volatile-rich late veneer with a CM chondritic composition (Wang and Becker, 2013) with 350 ng/g Cd is assumed (Wasson and Kallemeyn, 1988). In contrast, a volatile depleted late veneer with a composition akin to CO and EL chondrites would supply only 4.9 ± 0.8% of the BSE Cd inventory, even for a large late veneer equivalent to 3% M_E and (Fig. 4, Table 3). In this case, the BSE budget of Cd, and other similarly volatile elements, is almost exclusively delivered during the main stage of accretion, whilst core formation is still ongoing.

As our modelling infers that a chondritic late veneer is isotopically heavier in Cd than the BSE, larger additions of volatile-rich late veneer material must be balanced by main accretionary components that have increasingly lighter Cd isotope compositions (Figs. 4, 5, Table 3). In detail, for a 3% M_E late veneer with a volatile-poor CO-EL composition, the main stage accretion material can have a Cd isotope composition (of $\delta^{114}Cd = -0.08 \pm 0.10$) that is isotopically identical to the BSE, which features $\delta^{114}Cd_{BSE} = -0.06 \pm 0.06$ (Table 2). In contrast, a 3% M_E late veneer with a volatile-rich CI-EH composition requires main stage accretion material with a δ^{114}Cd value of −13.9 ± 13.3‰ (Figs. 4, 5, Table 3). Notably, the inferred light Cd isotope compositions are generally far removed from the δ^{114}Cd values of between about +0.2 and +0.5‰ that were determined for carbonaceous and enstatite chondrites (Fig. 5; Baker et al., 2010, Palk et al., 2018). Whilst previous studies also obtained δ^{114}Cd values outside of this range for some chondrites (Wombacher et al., 2003; Wombacher et al., 2008; Baker et al., 2010; Palk et al., 2018), such results most likely reflect Cd redistribution by thermal and shock metamorphism on the parent bodies and they are hence unlikely to be representative of the bulk asteroids.

5.2.4. Modelling formation of a Hadean matte

O'Neill (1991) proposed that the siderophile element abundances of the BSE may record separation of an immiscible sulphide phase, termed the 'Hadean matte' (HM), from the mantle near the end of accretion but before the delivery of the late veneer. In accord with this interpretation, Savage et al. (2015) concluded that the difference in the Cu isotope compositions inferred for the mantle and the bulk Earth may reflect segregation of a sulphide-rich phase during accretion. Laurenz et al. (2016) were furthermore able to reproduce mantle HSE and sulphur concentrations through a combination of late-stage sulphide segregation and subsequent addition of a ~ 0.4% M_E late veneer. Because Cd partitioning, and possibly Cd isotope fractionation, are controlled by the presence of S in the metal phase, an additional 'Hadean matte' model was formulated that accounts for the Cd partitioning and isotope effects imparted on the BSE through the separation of a possible HM (Tables 2, 3). This model incorporates a second set of core formation calculations that follow Eqs. (9) and (10) and which represent sulphide segregation after main stage core formation but before the arrival of the late veneer. Assuming the HM contained 46 ± 8 wt% Fe and was characterised by an X_S value of 0.43 ± 0.09 (Table 2), a ln K_D of 1.5 ± 1.8 (2SE) is estimated from Eq. (6) for the segregation of the HM from the silicate mantle, which corresponds to a D_{Cd} of 33. The model also applies a $\Delta^{114}Cd_{sul\text{-}sil}$ value of −0.18 ± 0.04‰ for the Cd isotope fractionation between the HM and mantle to highlight the maximum potential impact that Cd isotope fractionation could have during sulphide segregation (Table 2).

Previous studies inferred that the HM represents ≤1.6% of Earth's core mass (Savage et al., 2015), corresponding to ≤0.8% of BSE mass. Given the relatively small mass estimated for a possible HM, and because Cd partitioning and isotope fractionation are only marginally different for sulphide-silicate versus metal-silicate equilibration, late sulphide segregation has only a minor impact on the Cd concentrations and isotope compositions that are inferred for Earth's main stage accretion materials (Table 3). In detail, accretion models that account for HM formation require main stage components that are about 25% more enriched in Cd than predicted by models that do not account for HM segregation and the results are still identical within error (Table 3). The HM models also require main stage accretion components with Cd isotope compositions that are on average only 0.05–0.3‰ lower in δ^{114}Cd than models with no HM. Importantly, these results are for a scenario that applies maximum estimates for $\Delta^{114}Cd_{sul\text{-}sil}$ and the size of the HM. Considering this, it is likely that late segregation of a possible HM had only a limited impact on the elemental and isotope partitioning of Cd during terrestrial accretion, and the Cd isotope constraints that follow from the standard accretion model still stand (Table 3).

5.2.5. Implications of the Cd accretion modelling

The experiments of this study demonstrate that no significant Cd isotope fractionation occurs during metal-silicate segregation (Fig. 2, Table 1). This implies that the light Cd isotope composition of the BSE relative to carbonaceous and enstatite chondrites (Pickard et al., 2022) is not a consequence of core formation, regardless of whether this encompasses segregation of a HM or not. Volatilisation of Cd is also an unlikely cause, as this would have likely taken place under kinetic control with only limited back-reaction, thereby producing a silicate Earth enriched in heavy Cd isotopes, which is not observed. It is possible, however, that the discrepancy in the δ^{114}Cd values of the BSE versus carbonaceous and enstatite chondrites is an artefact of the limited high precision Cd isotope data currently available for these meteorites, as the few published results may biased toward high δ^{114}Cd values. Alternatively, Earth's main stage of accretion and/or the late veneer encompassed material with a Cd isotope composition that was lighter compared to known carbonaceous and enstatite chondrite groups as well as possibly the BSE (Figs. 4, 5, Table 3).

Our accretion modelling is in accord with the conclusions of Albarède (2009) and Ballhaus et al. (2013), who inferred that a large (> 2% M_E) late veneer of volatile-rich CI material would provide the majority of the BSE inventory of strongly volatile elements with 50% condensation temperatures of between 500 and 800 K, including Cd, Pb and Zn. However, such a large late veneer would also supply HSE (e.g., Pd, Os, Ir, Pt) at abundance levels that exceed the BSE concentrations by

more than a factor of x3 (Wood et al., 2010). Furthermore, if more than about 65% of the BSE Cd budget is sourced from a CI-EH late veneer, this would require Earth's main stage accretion material to be characterised by a mean δ^{114}Cd of at most −0.5‰ and possibly substantially lower (Figs. 4, 5). Notably, the latter values are clearly lower than the δ^{114}Cd data available for carbonaceous and enstatite chondrites thought to be unaffected by Cd redistribution during parent body metamorphism (Wombacher et al., 2008; Baker et al., 2010; Palk et al., 2018). The same conclusion may also extend to the ordinary chondrites but their compositions are less well constrained, as the data are less precise and Cd isotope fractionations from metamorphism are more prominent (Wombacher et al., 2008). This discrepancy does not arise if a late veneer of volatile-depleted material akin to CO-EL chondrites is added to the BSE. However, even a large CO-EL-like late veneer of 3% M_E provides only about 5% of the BSE Cd inventory and will thus have only a minor impact on the volatile budgets of the BSE (Figs. 4, 5, Table 3).

Whilst accretion of a large late veneer of >2% M_E is, in principle, possible, the addition of a smaller late veneer is a more likely scenario because this does not supply an overabundance of HSE and require main stage accretion material with a δ^{114}Cd value far removed from those measured for carbonaceous and enstatite chondrites (Figs. 4, 5). These findings are in accord with classical models of accretion, which suggest that the majority of Earth's volatiles were added during main stage growth whilst core formation was still active and in line with observations that siderophile volatile elements are depleted in the BSE relative to lithophile elements of similar volatility because the former were additionally depleted by partitioning into Earth's core (Wood et al., 2010). Whilst metal-silicate partitioning of Cd appears to be largely independent of temperature and pressure, the partitioning data for other elements, as well as isotope and trace element studies, argue for heterogeneous accretion, whereby volatiles were primarily added during the last 10–20% of Earth's main accretion phase, most likely through addition of volatile-rich carbonaceous matter (Schönbächler et al., 2010; Wade et al., 2012; Mahan et al., 2018; Braukmüller et al., 2019; Budde et al., 2019; Righter et al., 2020; Kubik et al., 2021). The evidence available from most abundance and isotope studies of HSE and strongly siderophile volatile elements (particularly Se, Te) furthermore indicates that a small late veneer of <1% M_E and with a composition akin to CI or CM chondrites was added to Earth after completion of core formation. This scenario of volatile accretion is also in accord with the Cd accretion model of the present study, which highlights that even a small volatile-rich late veneer has a considerable impact on the BSE budget of Cd and, by inference, the silicate Earth inventories of other highly volatile elements that do not partition strongly into the core. In the context of such an accretion scenario, our Cd modelling indicates a bulk Earth composition with about 30 to 130 ng/g Cd and a δ^{114}Cd value of between about 0 and − 0.3‰ (Table 3). It will be of interest for future studies to investigate whether the distinctly light Cd isotope compositions determined for the BSE and inferred for the bulk Earth relative to carbonaceous and enstatite chondrites reflect volatile addition by material related to ordinary chondrites, as these are presently not sufficiently characterised to rule out such a contribution.

6. Conclusions

Metal-silicate partitioning experiments were carried out at 1.5 GPa and 1508 to 1843 K to better constrain Cd partitioning and isotope fractionation during core formation. At these conditions, there was no significant Cd stable isotope fractionation during the partitioning of Cd between metal and silicate phases with $\Delta^{114}Cd_{met\text{-}sil} = -0.02 \pm 0.09$‰ (2SD, $n = 7$). Whilst a Cd isotope fractionation of -0.23 ± 0.07‰ (2SE) was determined for Cd partitioning between the sulphide and silicate phases of one experiment, this was observed for a short run, where the phases may not have reached full equilibrium. Together, these findings suggest that Cd isotope fractionation during segregation of Earth's core was either absent or very minor.

The Cd partitioning data from the experiments of this and previous investigations were combined through multiple linear regression to better constrain Cd metal-silicate partitioning during terrestrial core formation. These analyses show that temperature and pressure have no statistically significant effect on Cd metal-silicate partitioning. Instead, Cd partitioning is primarily dependent on the molar fractions of S, C and Si in the metal phase. Use of the multiple linear regression, and a recent estimate for the composition of Earth's core, suggest that Cd is preferentially partitioned into the silicate phase during core formation, with a D_{Cd} of about 0.4 calculated for single-stage core formation. However, the light element composition of Earth's core, which strongly impacts D_{Cd}, is still a topic of intense debate. As such, D_{Cd} values larger than 1 cannot be ruled out at present for core formation, in accord with other evidence, which suggests that Cd is enriched in the core relative to the BSE.

The new results of this study and available data on the composition of the BSE and chondritic meteorites were applied in mass balance calculations to constrain the Cd signature of Earth's main stage accretion components prior to delivery of the late veneer. The modelling indicates Earth's main stage of accretion involved material with an average δ^{114}Cd that was lower than that of known carbonaceous and enstatite chondrites. Most likely, this reflects either poor characterisation of these chondritic meteorites by the relatively few high precision data currently available or that volatile delivery involved a significant fraction of material with a lighter Cd isotope composition compared to known carbonaceous and enstatite chondrites. Accretion models with larger masses of a volatile-rich late veneer require main stage accretion materials that have increasingly lower δ^{114}Cd values, and which hence differ more and more from previously analysed carbonaceous and enstatite chondrites that are unaffected by Cd isotope fractionations imparted by parent body metamorphism. This suggests that terrestrial accretion most likely did not encompass addition of a >2% M_E late veneer of CI chondritic composition, further supporting classical accretion models which invoke that volatile delivery occurred primarily during main stage accretion, alongside core formation.

Author contributions

HP: interpretation of results, including code development, data analysis, modelling; preparation of manuscript and support of revision. EP: Determination of Cd concentrations and isotope compositions including sample preparation, data analysis, validation; preliminary interpretation of results; data curation. BJW: Conceptualization of study; partitioning experiments and electron microprobe measurements; support of data interpretation, manuscript preparation and revision; funding acquisition. MR: Conceptualization of study, support of data interpretation, initial modelling and manuscript preparation; manuscript revision including code development and modelling; supervision, project management and funding acquisition.

Declaration of Competing Interest

The authors declare that they have no known competing financial interests or personal relationships that could have appeared to influence the work reported in this paper.

Data availability

All relevant research data are published in the article.

Acknowledgements

Katharina Kreissig, Barry Coles and the other members of the MAGIC Team are thanked for their help in keeping the clean labs and mass spectrometers running smoothly. Rayssa Martins provided support with the Monte Carlo modelling whilst Paul Savage and Adrian Muxworthy

supplied very helpful suggestions on an early version of the text. Further constructive comments by three anonymous referees and editor Catherine Chauvel significantly improved the manuscript. The research was supported by STFC research grants to BJW (ST/R000999/1) and MR (ST/N000803/1, ST/W001179/1) as well as STFC quota studentships to HR and EP.

Appendix A. Supplementary data

Supplementary data to this article can be found online at https://doi.org/10.1016/j.chemgeo.2022.121293.

References

Abouchami, W., Galer, S.J.G., Horner, T.J., Rehkämper, M., Wombacher, F., Xue, Z., Lambelet, M., Gault-Ringold, M., Stirling, C.H., Schönbächler, M., Shiel, A.E., Weis, D., Holdship, P.F., 2013. A common reference material for cadmium isotope studies - NIST SRM 3108. Geostand. Geoanal. Res. 37, 5–17.

Albarède, F., 2009. Volatile accretion history of the terrestrial planets and dynamic implications. Nature 461, 1227–1233.

Arnold, T., Schönbächler, M., Rehkämper, M., Dong, S., Zhao, F.-J., Kirk, G.J.D., Coles, B. J., Weiss, D.J., 2010. Determination of zinc stable isotope compositions in geological and biological samples by double spike MC-ICPMS. Anal. Bioanal. Chem. 398, 3115–3125.

Baker, R.G.A., Schönbächler, M., Rehkämper, M., Williams, H.M., Halliday, A.N., 2010. The thallium isotope composition of carbonaceous chondrites — New evidence for live 205Pb in the early solar system. Earth Planet. Sci. Lett. 291, 39–47.

Ballhaus, C., Laurenz, V., Münker, C., Fonseca, R.O.C., Albarède, F., Rohrbach, A., Lagos, M., Schmidt, M.W., Jochum, K.-P., Stoll, B., Weis, U., Helmy, H.M., 2013. The U/Pb ratio of the Earth's mantle—a signature of late volatile addition. Earth Planet. Sci. Lett. 362, 237–245.

Braukmüller, N., Wombacher, F., Hezel, D.C., Escoube, R., Münker, C., 2018. The chemical composition of carbonaceous chondrites: Implications for volatile element depletion, complementarity and alteration. Geochim. Cosmochim. Acta 239, 17–48.

Braukmüller, N., Wombacher, F., Funk, C., Münker, C., 2019. Earth's volatile element depletion pattern inherited from a carbonaceous chondrite-like source. Nat. Geosci. 12, 564–568.

Bridgestock, L.J., Williams, H., Rehkämper, M., Larner, F., Giscard, M.D., Hammond, S., Coles, B., Andreasen, R., Wood, B.J., Theis, K.J., Smith, C.L., Benedix, G.K., Schönbächler, M., 2014. Unlocking the zinc isotope systematics of iron meteorites. Earth Planet. Sci. Lett. 400, 153–164.

Budde, G., Burkhardt, C., Kleine, T., 2019. Molybdenum isotopic evidence for the late accretion of outer Solar System material to Earth. Nat. Astron. 3, 736–741.

Chou, C.-L., 1978. Fractionation of siderophile elements in the Earth's upper mantle. In: Proc. Lunar Planet. Sci. Conf., IX, pp. 219–230.

Dauphas, N., 2017. The isotopic nature of the Earth's accreting material through time. Nature 541, 521–524.

Fischer-Gödde, M., Kleine, T., 2017. Ruthenium isotopic evidence for an inner Solar System origin of the late veneer. Nature 541, 525–527.

Fischer-Gödde, M., Elfers, B.-M., Münker, C., Szilas, K., Maier, W.D., Messling, N., Morishita, T., Van Kranendonk, M., Smithies, H., 2020. 'Ruthenium isotope vestige of Earth's pre-late-veneer mantle preserved in Archaean rocks. Nature 579, 240–244.

Gudfinnsson, G.H., Presnall, D.C., 2000. Melting Behaviour of Model Lherzolite in the System CaO–MgO–Al_2O_3–SiO_2–FeO at 0·7–2·8 GPa. J. Petrol. 41, 1241–1269.

Guinoiseau, D., Galer, S.J.G., Abouchami, W., 2018. Effect of cadmium sulphide precipitation on the partitioning of Cd isotopes: Implications for the oceanic Cd cycle. Earth Planet. Sci. Lett. 498, 300–308.

Heber, V.S., Brooker, R.A., Kelley, S.P., Wood, B.J., 2007. Crystal–melt partitioning of noble gases (helium, neon, argon, krypton, and xenon) for olivine and clinopyroxene. Geochim. Cosmochim. Acta 71, 1041–1061.

Hellmann, J.L., Hopp, T., Burkhardt, C., Becker, H., Fischer-Gödde, M., Kleine, T., 2021. Tellurium isotope cosmochemistry: Implications for volatile fractionation in chondrite parent bodies and origin of the late veneer. Geochim. Cosmochim. Acta 309, 313–328.

Holzheid, A., Sylvester, P., O'neill, H.S.C., Rubie, D.C., Palme, H., 2000. Evidence for a late chondritic veneer in the Earth's mantle from high-pressure partitioning of palladium and platinum. Nature 406, 396–399.

Hopp, T., Budde, G., Kleine, T., 2020. Heterogeneous accretion of Earth inferred from Mo-Ru isotope systematics. Earth Planet. Sci. Lett. 534, 116065.

Jacobson, S.A., Morbidelli, A., Raymond, S.N., O'brien, D.P., Walsh, K.J., Rubie, D.C., 2014. Highly siderophile elements in Earth's mantle as a clock for the Moon-forming impact. Nature 508 (7494), 84–87.

Kiseeva, E.S., Wood, B.J., 2013. A simple model for chalcophile element partitioning between sulphide and silicate liquids with geochemical applications. Earth Planet. Sci. Lett. 383, 68–81.

Kiseeva, E.S., Wood, B.J., 2015. The effects of composition and temperature on chalcophile and lithophile element partitioning into magmatic sulphides. Earth Planet. Sci. Lett. 424, 280–294.

Kubik, E., Siebert, J., Blanchard, I., Agranier, A., Mahan, B., Moynier, F., 2021. Earth's volatile accretion as told by Cd, Bi, Sb and Tl core–mantle distribution. Geochim. Cosmochim. Acta 306, 263–280.

Lagos, M., Ballhaus, C., Münker, C., Wohlgemuth-Ueberwasser, C., Berndt, J., Kuzmin, D. V., 2008. The Earth's missing lead may not be in the core. Nature 456, 89–92.

Laurenz, V., Rubie, D.C., Frost, D.J., Vogel, A.K., 2016. The importance of sulfur for the behavior of highly-siderophile elements during Earth's differentiation. Geochim. Cosmochim. Acta 194, 123–138.

Lodders, K., Fegley, B.J., 1998. The Planetary Scientist's Companion. Oxford University Press, New York.

Mahan, B., Siebert, J., Pringle, E.A., Moynier, F., 2017. Elemental partitioning and isotopic fractionation of Zn between metal and silicate and geochemical estimation of the S content of the Earth's core. Geochim. Cosmochim. Acta 196, 252–270.

Lorand, J.-P., Conquéré, F., 1983. Contribution à l'étude des sulfures dans les enclaves de lherzolite à spinelle des basaltes alcalins (Massif Central et Languedoc, France). Bull. Minéral. 106, 585–606.

Mahan, B., Siebert, J., Blanchard, I., Borensztajn, S., Badro, J., Moynier, F., 2018. Constraining compositional proxies for Earth's accretion and core formation through high pressure and high temperature Zn and S metal-silicate partitioning. Geochim. Cosmochim. Acta 235, 21–40.

Mann, U., Frost, D.J., Rubie, D.C., Becker, H., Audétat, A., 2012. Partitioning of Ru, Rh, Pd, Re, Ir and Pt between liquid metal and silicate at high pressures and high temperatures - Implications for the origin of highly siderophile element concentrations in the Earth's mantle. Geochim. Cosmochim. Acta 84, 593–613.

Marin, N., Righter, K., Danielson, L., Pando, K., Lee, C., 2013. Metal-silicate partitioning of Bi, In, and Cd as a function of temperature and melt compositio. In: 44th Lunar and Planetary Science Conference, The Woodlands, Texas, 18-22 March, #1848 (abstr.).

Meisel, T., Walker, R.J., Morgan, J.W., 1996. The osmium isotopic composition of the Earth's primitive upper mantle. Nature 383, 517–520.

Meisel, T., Walker, R.J., Irving, A.J., Lorand, J.-P., 2001. Osmium isotopic compositions of mantle xenoliths: a global perspective. Geochim. Cosmochim. Acta 65, 1311–1323.

Mills, K.C., Hayashi, M., Wang, L., Watanabe, T., 2014. The structure and properties of silicate slags. In: Seetharaman, S. (Ed.), Treatise on Process Metallurgy: Process Fundamentals. Elsevier, Amsterdam, pp. 149–286.

Murphy, K., Rehkämper, M., Kreissig, K., Coles, B., Van De Flierdt, T., 2016. Improvements in Cd stable isotope analysis achieved through use of liquid-liquid extraction to remove organic residues from Cd separates obtained by extraction chromatography. J. Anal. At. Spectrom. 31 (1), 319–327.

O'Neil, J.R., 1986. Theoretical and experimental aspects of isotopic fractionations. In: Valley, J.W., Taylor, J.R., O'Neil, J.R. (Eds.), Stable Isotopes in High Temperature Geological Processes. Mineralogical Society of America, Washington D.C., pp. 1–40

O'Neill, H.S.C., 1991. The origin of the Moon and the early history of the Earth – a chemical model. Part 2: the Earth. Geochim. Cosmochim. Acta 55, 1159–1172.

Palk, E., Andreasen, R., Rehkämper, M., Stunt, A., Kreissig, K., Coles, B., Schönbächler, M., Smith, C., 2018. Variable Tl, Pb, and Cd concentrations and isotope compositions of enstatite and ordinary chondrites – evidence for volatile element mobilization and decay of extinct ^{205}Pb. Meteorit. Planet. Sci. 53 (2), 167–186.

Palme, H., O'neill, H.S.C., 2014. Cosmochemical estimates of mantle composition. In: Holland, H.D., Turekian, K.K. (Eds.), Treatise on Geochemistry, 2nd ed. Elsevier, Amsterdam, pp. 1–39.

Palme, H., Lodders, K., Jones, A., 2014. Solar system abundances of the elements. In: Holland, H.D., Turekian, K.K. (Eds.), Treatise on Geochemistry, 2nd ed., pp. 15–36 Elsevier, Amsterdam.

Pickard, H., Palk, E., Schönbächler, M., Moore, R.E.T., Coles, B.J., Kreissig, K., Nilsson-KerR, K., Hammond, S.J., Takazawa, E., Hémond, C., Tropper, P., Barfod, D.N., Rehkämper, M., 2022. The cadmium and zinc isotope compositions of the silicate Earth – Implications for terrestrial volatile accretion. Geochim. Cosmochim. Acta 338, 165–180.

Presnall, D.C., Dixon, S.A., Dixon, J.R., O'donnell, T.H., Brenner, N.L., Schrock, R.L., Dycus, D.W., 1978. Liquidus phase relations on the join diopside-forsterite-anorthite from 1 atm to 20 kbar: their bearing on the generation and crystallization of basaltic magma. Contrib. Mineral. Petrol. 66, 203–220.

Righter, K., 2011. Prediction of metal–silicate partition coefficients for siderophile elements: an update and assessment of PT conditions for metal–silicate equilibrium during accretion of the Earth. Earth Planet. Sci. Lett. 304, 158–167.

Righter, K., Pando, K., Marin, N., Ross, D.K., Righter, M., Danielson, L., Lapen, T.J., Lee, C., 2018. Volatile element signatures in the mantles of Earth, Moon, and Mars: Core formation fingerprints from Bi, Cd, In, and Sn. Meteorit. Planet. Sci. 53, 284–305.

Righter, K., Pando, K., Ross, D.K., Righter, M., Lapen, T.J., 2019. Effect of silicon on activity coefficients of Bi, Cd, Sn, and Ag in liquid Fe-Si, and implications for differentiation and core formation. Meteorit. Planet. Sci. 54 (6), 1379–1394.

Righter, K., Schönbächler, M., Pando, K., Rowland, R., Righter, M., Lapen, T., 2020. Ag isotopic and chalcophile element evolution of the terrestrial and martian mantles during accretion: New constraints from Bi and Ag metal-silicate partitioning. Earth Planet. Sci. Lett. 552, 116590.

Ripperger, S., Rehkämper, M., 2007. Precise determination of cadmium isotope fractionation in seawater by double spike MC-ICPM. Geochim. Cosmochim. Acta 71, 631–642.

Savage, P.S., Moynier, F., Chen, H., Shofner, G., Siebert, J., Badro, J., Puchtel, I.S., 2015. Copper isotope evidence for large-scale sulphide fractionation during Earth's differentiation. Geochemical Perspectives Letters 1, 53–64.

Schmitt, A.-D., Galer, S.J.G., Abouchami, W., 2009. Mass-dependent cadmium isotopic variations in nature with emphasis on the marine environment. Earth Planet. Sci. Lett. 277, 262–272.

Schönbächler, M., Carlson, R.W., Horan, M.F., Mock, T.D., Hauri, E.H., 2010. Heterogeneous accretion and the moderately volatile element budget of Earth. Science 328, 884–887.
Steenstra, E.S., Lin, Y., Dankers, D., Rai, N., Berndt, J., Matveev, S., van Westrenen, W., 2017. The lunar core can be a major reservoir for volatile elements S, Se, Te and Sb. Scientific Reports 7, 14552.
Steenstra, E.S., Berndt, J., Klemme, S., Fei, Y., Van Westrenen, W., 2020a. A possible high-temperature origin of the Moon and its geochemical consequences. Earth Planet. Sci. Lett. 538, 116222.
Steenstra, E.S., Seegers, A.X., Putter, R., Berndt, J., Klemme, S., Matveev, S., Bullock, E. S., Van Westrenen, W., 2020b. Metal-silicate partitioning systematics of siderophile elements at reducing conditions: a new experimental database. Icarus 335, 113391.
Tuff, J., Wood, B.J., Wade, J., 2011. The effect of Si on metal–silicate partitioning of siderophile elements and implications for the conditions of core formation. Geochim. Cosmochim. Acta 75, 673–690.
Varas-Reus, M.I., König, S., Yierpan, A., Lorand, J.P., Schoenberg, R., 2019. Selenium isotopes as tracers of a late volatile contribution to Earth from the outer Solar System. Nat. Geosci. 12, 779–782.
Wade, J., Wood, B.J., Tuff, J., 2012. Metal–silicate partitioning of Mo and W at high pressures and temperatures: evidence for late accretion of sulphur to the Earth. Geochim. Cosmochim. Acta 85, 58–74.
Walker, R.J., 2009. Highly siderophile elements in the Earth, Moon and Mars: Update and implications for planetary accretion and differentiation. Geochemistry 69, 101–125.
Walter, M.J., Presnall, D.C., 1994. Melting behavior of simplified lherzolite in the system CaO-MgO-Al_2O_3-SiO_2-Na_2O from 7 to 35 kbar. J. Petrol. 35, 329–359.
Wang, Z., Becker, H., 2013. Ratios of S, Se and Te in the silicate Earth require a volatile-rich late veneer. Nature 499, 328–331.
Wang, Z., Laurenz, V., Petitgirard, S., Becker, H., 2016. Earth's moderately volatile element composition may not be chondritic: evidence from In, Cd and Zn. Earth Planet. Sci. Lett. 435, 136–146.
Wang, H.S., Lineweaver, C.H., Ireland, T.R., 2018. The elemental abundances (with uncertainties) of the most Earth-like planet. Icarus 299, 460–474.
Wänke, H., 1981. Constitution of terrestrial planets. Phil. Trans. R. Soc. Lond. A 303, 287–302.
Wasson, J.T., Kallemeyn, G.W., 1988. Compositions of chondrites. Phil. Trans. R. Soc. Lond. A 325, 535–544.
Wombacher, F., Rehkämper, M., Mezger, K., Münker, C., 2003. Stable isotope compositions of cadmium in geological materials and meteorites determined by multiple-collector ICPMS. Geochim. Cosmochim. Acta 67, 4639–4654.
Wombacher, F., Rehkämper, M., Mezger, K., Bischoff, A., Münker, C., 2008. Cadmium stable isotope cosmochemistry. Geochim. Cosmochim. Acta 72, 646–667.
Wood, B.J., Nielsen, S.G., Rehkämper, M., Halliday, A.N., 2008. The effects of core formation on the Pb- and Tl- isotopic composition of the silicate Earth. Earth Planet. Sci. Lett. 269, 326–336.
Wood, B.J., Halliday, A.N., Rehkämper, M., 2010. Volatile accretion history of the Earth. Nature 467, E6–E7.
Wood, B.J., Kiseeva, E.S., Mirolo, F.J., 2014. Accretion and core formation: the effects of sulfur on metal–silicate partition coefficients. Geochim. Cosmochim. Acta 145, 248–267.
Wood, B.J., Smythe, D.J., Harrison, T., 2019. The condensation temperatures of the elements: a reappraisal. Am. Mineral. 104, 844–856.
Xie, R.C., Rehkämper, M., Grasse, P., Van De Flierdt, T., Frank, M., Xue, Z., 2019. Isotopic evidence for complex biogeochemical cycling of Cd in the eastern tropical South Pacific. Earth Planet. Sci. Lett. 512, 134–146.
Xue, Z., Rehkämper, M., Schönbächler, M., Statham, P.J., Coles, B.J., 2012. A new methodology for precise cadmium isotope analyses of seawater. Anal. Bioanal. Chem. 402, 883–893.
Young, E.D., Kohl, I.E., Warren, P.H., Rubie, D.C., Jacobson, S.A., Morbidelli, A., 2016. Oxygen isotopic evidence for vigorous mixing during the Moon-forming giant impact. Science 351, 493–496.